Eng. Sci., 2025, **35**, 1501

Engineered Science
DOI: https://dx.doi.org/10.30919/es1501

Manganese Dioxide/Nickel Cobalt Layered Double Hydroxide Composite Electrodes for Asymmetric Supercapacitors

Hong Gao[1] and Yong Ma[2,*]

Abstract

At present, the low energy density poses a challenge that hinders the advancement and use of supercapacitors. Selecting appropriate techniques to enhance the performance of electrode materials is a viable approach, and designing these materials is crucial. This study involves the chemical deposition of a manganese dioxide (MnO_2) nanosheet layer onto activated carbon cloth (CF), followed by the electrochemical deposition of a cobalt-nickel layered double hydroxide (CoNi LDH) layer on the former, giving rise to the creation of the CF/MCN electrode. This bilayer heterostructure can effectively exploit the synergistic effect of different materials and provide more excellent electrochemical performance. The constructed asymmetric supercapacitor of CF/MCN//activated carbon (AC), demonstrated 1.6 V voltage range, 151 F g^{-1} specific capacitance at 1 A g^{-1}, and 53.69 W h kg^{-1} energy density at 800.02 W kg^{-1} power density. Moreover, following 10,000 cycles, the device exhibits 90.35% capacitance retention as well as approaches nearly 100% coulombic efficiency. The device demonstrates significant potential for application in the realm of innovative energy technologies. This research contributes novel insights that may enhance the structural design of electrode materials for future generations of supercapacitors.

Keywords: MnO_2; CoNi LDH; Asymmetric supercapacitor; Electrochemical performances.
Received: 25 March 2025; Revised: 15 April 2025; Accepted: 01 May 2025.
Article type: Research article.

1. Introduction

The advancement of secure, environmentally friendly, high-efficient, along with associated energy storage technologies, holds significant relevance in contemporary discourse.[1,2] Supercapacitors integrate the beneficial characteristics of both batteries and capacitors, exhibiting high power density, rapid charge and discharge capabilities, and exceptional recyclability.[3] These attributes render them highly appropriate for a diverse array of applications.[4] At present, supercapacitors are divided into different types, symmetrical supercapacitors,[5] and asymmetric supercapacitors, which have shown amazing performance in different application directions, such as the field of flexible energy devices and the medical field.[6-8] The electrodes of supercapacitors are critical components in the charge storage process, significantly influencing electrochemical properties of supercapacitor system.[9] Choosing and crafting the appropriate materials is crucial for boosting the performance, unlocking their true abilities as the next wave of energy storage innovation.

Double hydroxide has a layered or porous structure and therefore possesses a significant specific surface area, facilitating the adsorption and storage of charge, thus increasing the specific capacitance of supercapacitors.[10-12] With abundant redox activity, they are capable of rapid electron and ion transfer during electrochemical processes, providing efficient charge storage and release capabilities. By means of synthesis methods, doping compositions, and structural modulation, it is possible to achieve the adjustment of the structural characteristics and properties of double hydroxide compounds to address the requirements of various application scenarios.[13,14] Moreover, the raw materials of double hydroxides are usually easy to obtain and low cost, and some double hydroxides are even naturally occurring, which is environmentally friendly.[15] However, it was found during the research process that it has the disadvantage of easy agglomeration, which seriously affects its further use.[16]

A large number of research scholars have done some work to address these two shortcomings. Li *et al.*[17] developed three-dimensional hierarchical $NiCo_2O_4$@NiCo-layered double hydroxide (LDH) core-shell structures on utilizing a straightforward hydrothermal method followed by an

[1] *Sino-german School of Engineering, Qingdao University of Science and Technology, Qingdao, 266590, China*
[2] *School of Material Science and Engineering, Shandong University of Science and Technology, Qingdao, 266590, China*
**Email:* mayong@sdust.edu.cn (Y. Ma)

electrodeposition process. The $NiCo_2O_4$ nanowires created a nanoarray framework onto the carbon cloth (CF), while the NiCo LDH provided a shell that enhanced the electrochemically active sites. This structure also established mesoporous stratified channels, which effectively facilitated the movement of electrons and ions. The core-shell architecture enhanced the face capacitance, achieving a value of 6092 mF cm^{-2}. A capacitance retention of 83.9% was attained following 5000 cycles at 30 mA cm^{-2}. Moreover, an asymmetric supercapacitor (ASC) had been constructed utilizing $NiCo_2O_4$@NiCo-LDH in conjunction with activated carbon (AC). This advanced supercapacitor exhibits 49 W h kg^{-1} energy density at 750 W kg^{-1} power density and sustains 30 W h kg^{-1} energy density at 7500 W kg^{-1} power density. Following 2000 cycles at 5 A g^{-1}, the initial capacitance retention of the ASC was recorded at 83.3%, showing good cycling stability. The notable enhancement in performances suggests the potentially applicable utilization of core-shell architecture when integrated with CF, which provides a basis for the design of novel ASC structures and the advancement of next-generation energy storage technologies.

Manganese dioxide (MnO_2) has abundant resources, elevated specific surface area, good electrochemical activity and stabilization and relatively lower cost, which makes it an ideal choice.[18-20] Its micro-nano structure provides a large amount of active surface area, which facilitates efficient charge transport and storage, resulting in elevated energy and high power density, as well as environmentally friendly and chemically stable characteristics, providing an important basis for the performance enhancement and application expansion of supercapacitors.[21-24] Meanwhile, the advantage of its regular shape can be used to improve the easy agglomeration phenomenon of CoNi LDH.

In this study, after MnO_2 with a layer of nano-flaky morphology was obtained by chemical deposition on an activated CF substrate, CoNi LDH was grown on the surface of MnO_2 by a simple electrochemical deposition technique. The resulting compact and regular CF/MCN electrodes were prepared by this method and published for the first time. The heterogeneous electrode material has the advantages of large specific surface area and abundant active sites, which speeds up the electrochemical reaction speed, has excellent specific capacitance, and improves the comprehensive electrochemical performance of the compound. AC is selected for negative electrode and assembled with CF/MCN to form an ACS device, which has good cycling stability and practical application value. This study presents a novel concept for the advancement of electrode materials within the domain of next-generation energy storage uses.

2. Experimental part

2.1 Reagents

All reagents were bought for immediate application, with the exception of CC refluxed at 100 °C for 5 h in a mixed solution of H_2SO_4 and HNO_3 (1:2) prior to use to enhance surface hydrophilicity.

2.2 Preparation of CF/MnO_2 electrode

Take 1.5 g $KMnO_4$, 150 mL distilled water, 0.5 mL concentrated H_2SO_4 configuration solution, add magnetons into the solution, stir magnetically for 10 min, and then add activated CF to the solution. The reaction was conducted in a water bath maintained at 85 °C for 90 min. After the reaction is completed, the beaker is taken out of the constant temperature water bath and allowed to cool to ambient temperature, and then the reacted CF is placed in the petri dish, sealed with plastic wrap and baked in the oven for 12 h, then the CF/MnO_2 electrode can be obtained.

2.3 Preparation of CF/MCN electrode

0.7 g $Co(NO_3)_2 \cdot 6H_2O$ and 1.4 g $(Ni(NO_3)_2 \cdot 6H_2O$ were dissolved in 30 mL H_2O to prepare a solution. The device composed of CF/MnO_2 electrode, mercury oxide reference electrode and platinum plate against electrode was put into the prepared solution and electrochemical deposition was carried out. A layer of CoNi LDH material was fabricated onto the outer periphery of CF/MnO_2 electrode via electrochemical deposition method (constant voltage -1 V, deposition 300 s), and finally the CF/MCN electrode was formed.

2.4 Preparation of CF/CoNi LDH electrode

In order to conduct a control test, a solution was prepared by dissolving 0.7 g $Co(NO_3)_2 \cdot 6H_2O$, 1.4 g $Ni(NO_3)_2 \cdot 6H_2O$, and 30 mL H_2O. And a device consisting of CF working electrode, mercury oxide reference electrode and platinum sheet electrode was put into the solution and connected to an electrochemical workstation. CF/CoNi LDH electrodes were prepared by electrochemical deposition (constant voltage -1 V, deposition 300 s).

2.5 Preparation of CF/AC electrode

A mixture comprising AC, PVDF and acetylene black (mass ratio: 8:1:1) is introduced to the mortar, and the mixture is uniform after a long time of grinding, and the black mixture is obtained. Then, it is evenly coated on the CF substrate, and then baked in the oven for about 10 hours, and finally the CF/AC electrode can be obtained.

2.6 Assembling of asymmetric supercapacitor

To emphasize practical importance of the CF/MCN electrode, a supercapacitor device with an asymmetric structure (MCN//AC) has been constructed, the gel electrolyte of PVA/KOH electrode and the non-woven fabric as the diaphragm.

2.7 Materials characterization and electrochemical measurements

The samples' microscopic structure was obtained using scanning electron microscopy (SEM, Hitachi S-4800) in conjunction with energy dispersive spectroscopy (EDS,

Hitachi S-4800). And their structure proceeded by X-ray diffraction (XRD, D8 ADVANCE Da Vinci), Fourier infrared spectroscopy (FTIR, Nicolet Avatar 370) and X-ray photoelectron spectroscopy (XPS, ESCALAB 250). The electrochemical properties of the electrodes and ASC were tested using the CHI660E electrochemical workstation. In the EIS test procedure, the frequency range was 0.01 Hz-100 kHz and the amplitude were 5 mV. The performance in repeated cycles of the ASC was characterized using the CT2001A blue electric test system.

3. Results and discussion

Fig. 1 shows the synthesis of CF/MCN electrodes. Firstly, a layer of nano-flaky MnO_2 is grown by chemical deposition on the activated CF surface. Because the activated CF surface has rich functional groups and active sites, MnO_2 can grow evenly on the surface of the CF. A layer of CoNi LDH has been applied to the surface of MnO_2 by electrodeposition to obtain electrode material with heterogeneous structure. The presence of the MnO_2 increases the voltage window of the entire compound and prevents the outer layer of the LDH from flaking, and the presence of CoNi LDH can significantly enhance the specific capacitance of the resulting electrode.

The surface morphology of CF/MnO_2 and CF/MCN is analyzed through SEM (Fig. 2). Figs. 2 (a-c) demonstrate the shape of CF/MnO_2 surface with uniform distribution of surface holes. MnO_2 nanoflake structures measuring approximately 0.71 μm in height are uniformly dispersed across the CF/MnO_2 surface, which clearly indicate the success in-situ synthesis of MnO_2 on CF. The holes in the surface of the resulting samples are distinctly observable in the enlarged representation depicted by Fig. 2(c). Figs. 2(d-f) illustrate the structure of CF/MCN, which is significantly different compared to CF/MnO_2. This difference highlights the effective encapsulation of the MnO_2 substrate by the outermost CoNi LDH material. This combination results in a composite structure with a diameter of 10.62 μm. Figs. 2(e-f) provide clearer images of CF/MCN, revealing uniformly arranged nanosheets in the outermost layer, which are riddled with holes. This structural feature contributes to enhanced electrolyte penetration and thus helps to improve electrochemical properties.

Fig. 2(g) shows a specially chosen case of CF/MC with elemental mapping to depict the elemental composition within the material. Figs. 2(h-1) show C, Mn, Co, Ni and O in CF/MCN. It is evident that the distribution of the C element across the scanning plane is attributable to the existence of CF. Due to the presence of MnO_2, the Mn element is widely distributed in the plane, indicating that MnO_2 has been fully synthesized. The almost duplicated distribution of Co and Ni elements serves as evidence for the successful synthesis of the CoNi LDH. The distribution of O element across planar surface is observed to be more pronounced in regions where with the CF.

The element composition and surface electronic valence of CF/MCN are subjected to XPS.[25,26] The detection of C, Mn, Co, O, and Ni presented in Fig. 3(a) aligns with the findings obtained from EDS. From Fig. 3(b), the C 1s spectrum characterized by three distinct peaks is seen, at 284.8, 285.9, 288.6 eV and these peaks are in correspondence with C-C, C-

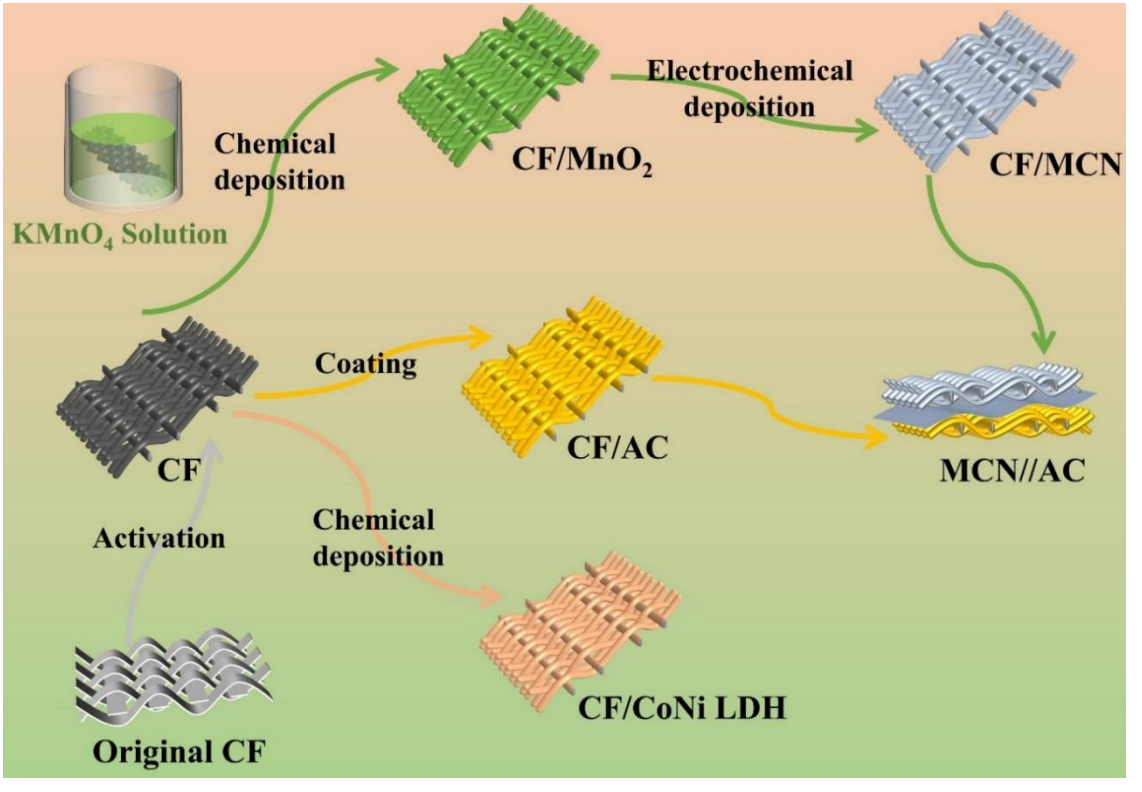

Fig. 1: Schematic representation of MCN//AC synthesis.

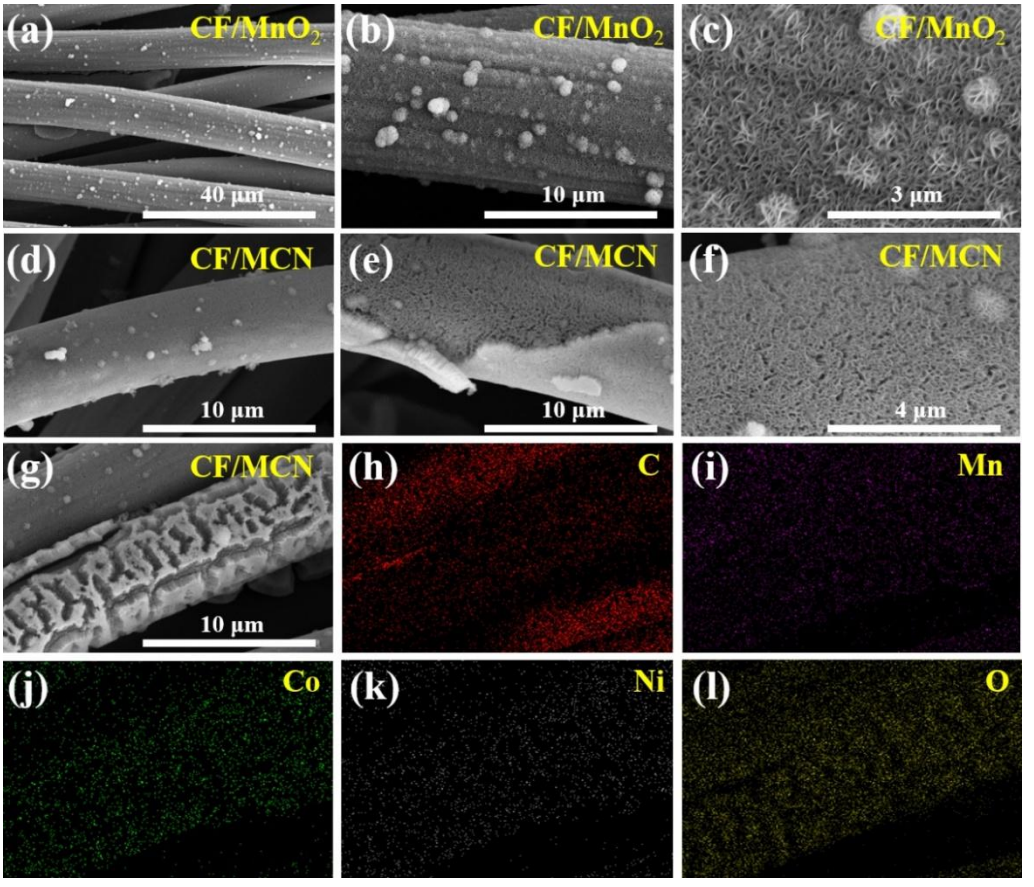

Fig. 2: SEM images of (a-c) CF/MnO_2 and (d-f) CF/MCN, (g-l) elemental mapping for CF/MCN including C, Mn, Co, Ni, O.

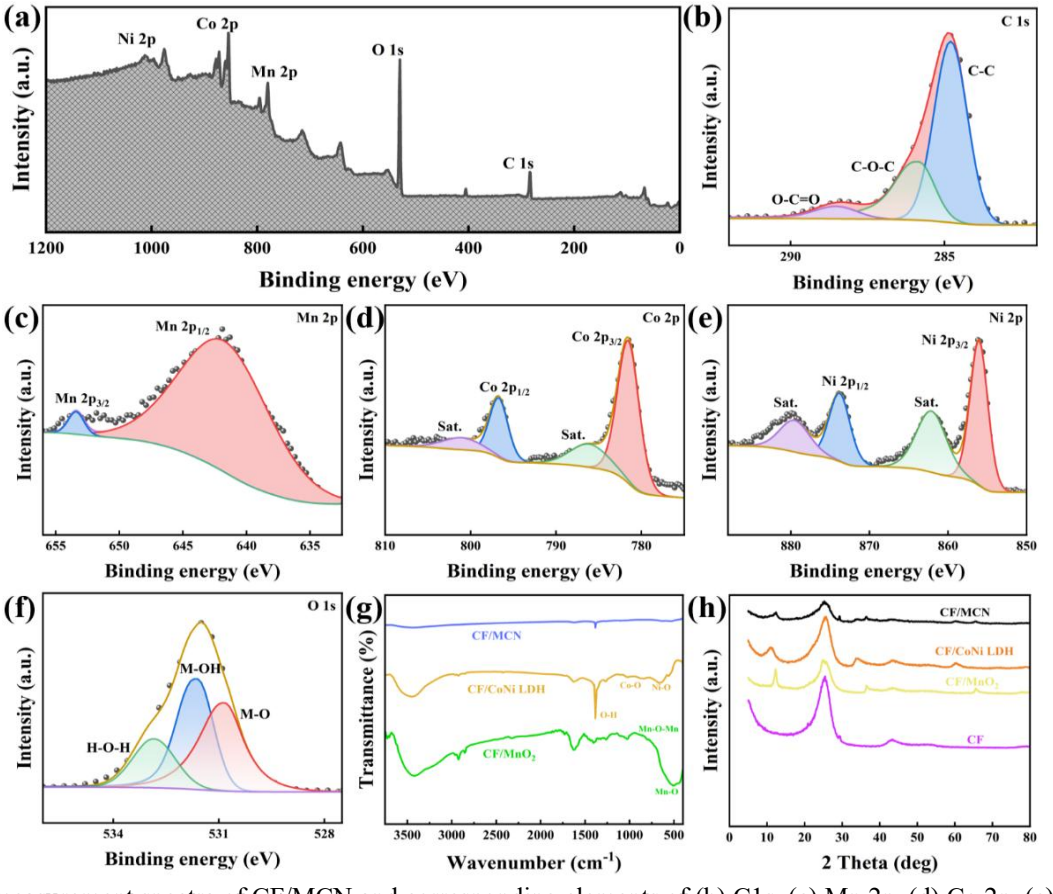

Fig. 3: (a) XPS measurement spectra of CF/MCN and corresponding elements of (b) C1s, (c) Mn 2p, (d) Co 2p, (e) Ni 2p, (f) O 1s, (g) FTIR spectra of CF/MnO_2, CF/CoNi LDH, CF/MCN, (h) XRD patterns of CF, CF/MnO_2, CF/CoNi LDH, CF/MCN.

Co and Ni elements appear, thereby providing additional evidence of the effective integration of these two materials O-C, O-C=O in sequence. From Fig. 3(c), two peaks can be seen in Mn 2p at 653.4 and 642.3 eV, aligning with the Mn $2p_{3/2}$ and Mn $2p_{1/2}$ peaks in that order. Energy gap between them is 11.1 eV, which suggests the existence of MnO_2.[27] The fitting of the Co 2p peak, as illustrated in Fig. 3(d), shows two spin-orbit bimodal peaks corresponding to Co $2p_{3/2}$ and Co $2p_{1/2}$ at 781.5 eV for Co $2p_{3/2}$ and 796.8 eV for Co $2p_{1/2}$, and the two satellite peaks are at 786.1 and 801.1 eV, respectively.[28,29] From Fig. 3(e), two major peaks can be found in the Ni 2p spectrum.[30] A set of two peaks at 856.2 and 873.9 eV relating to the signals at Ni $2p_{3/2}$ and Ni $2p_{1/2}$, and satellite peaks corresponding to two oscillating satellite peaks at 862.2 and 879.4 eV, respectively.[31] In Fig. 3(f), the O 1s spectrum is featured d by three distinct peaks at 530.8, 531.7, 532.9 eV, which are attributed to the presence of M-O, M-OH (M represents Co or Ni), H-O-H, one by one.

Fig. 3(g) presents the FTIR spectra for CF/MnO_2, CF/CoNi LDH and CF/MCN. The peaks of CF/MnO_2 at 809 and 518 cm^{-1} are caused by Mn-O-Mn and Mn-O tensile vibrations. For CF/CoNi LDH, the peaks observed at 1022 and 665 cm^{-1} are assigned to Co-O and Ni-O tensile vibrations within hydroxide structure, respectively.[32] Meticulous analysis reveals the presence of distinct peaks corresponding to the above mentioned two compounds within the spectra of CF/MCN, indicating that these substances still exist in CF/MCN, proving that CF/MCN has been successfully prepared. For investigating structural characteristics of the materials, XRD analyses are performed on CF, CF/MnO_2, CF/CoNi LDH, and CF/MCN, which is illustrated in Fig. 3(h). These materials exhibit analogous diffraction peaks at 25.1 and 43.2°, also serving as the characteristic peak of the carbon fibers. Besides, 12.4, 37.3 and 65.5° correspond to (100), (-111) and (002) crystal faces of MnO_2, respectively. The characteristic peaks of CF/CoNi LDH at 11.3, 33.5, and 59.9° relate to (003), (101), and (110) crystal faces of CoNi LDH, respectively.[10,11] The characteristic peaks of each single material are observable in XRD pattern of CF/MCN. This indicates that neither of these two heterogeneous layers is compromised in the course of synthesis, thereby demonstrating the successful fabrication of CF/MCN.[33,34]

Electrochemical performances of the fabricated electrodes are tested using the electrochemical analyses of CV, GCD and EIS with 1 mol L^{-1} KOH solution. Fig. 4 represents electrochemical analysis test of CF/MnO_2 electrode. Fig. 4(a) illustrates the CV curves of the CF/MnO_2-50 electrode with various scan rates. Comparison shows that the shape of the curve changes but not much when scan rate is elevated from 10-100 mV s^{-1}, suggesting an enhancement in electrochemical reversibility and an improved capacitance for rapid ion transport. In addition, the existence of notable redox peaks at 0.17 and 0.49 V suggests the emergence of a faradaic redox reaction, which plays a crucial role in enhancing the overall capacitance. Also with the three images in Figs. 4(c-g) analyzed, which represent the CV curves of CF/MnO_2-70, CF/MnO_2-90 and CF/MnO_2-110 electrodes, there are changes in the curve shapes though not substantial, indicating that they also have better electrochemical reversibility and rapid ion transport. Fig. 4(b) depicts the GCD curves of CF/MnO_2-50 under different current densities. The symmetry is shown to be less pronounced and the voltage plateau is smaller, indicating an average charge storage capacitance. Similarly, the three images in Figs. 4(d-h) are analyzed, which represent GCD

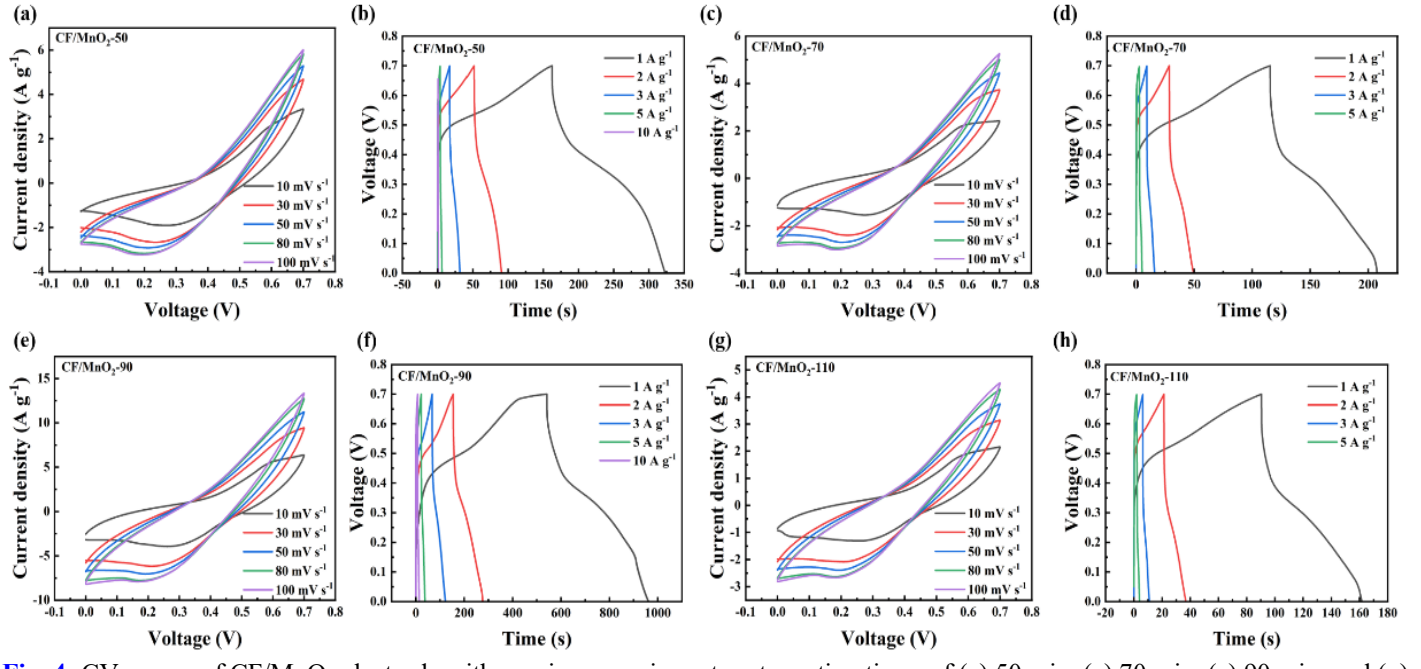

Fig. 4: CV curves of CF/MnO_2 electrode with varying scanning rates at reaction times of (a) 50 min, (c) 70 min, (e) 90 min, and (g) 110 min, respectively, GCD curves of CF/MnO_2 electrode under diverse current densities at (b) 50 min, (d) 70 min, (f) 90 min, and (h) 110 min, respectively.

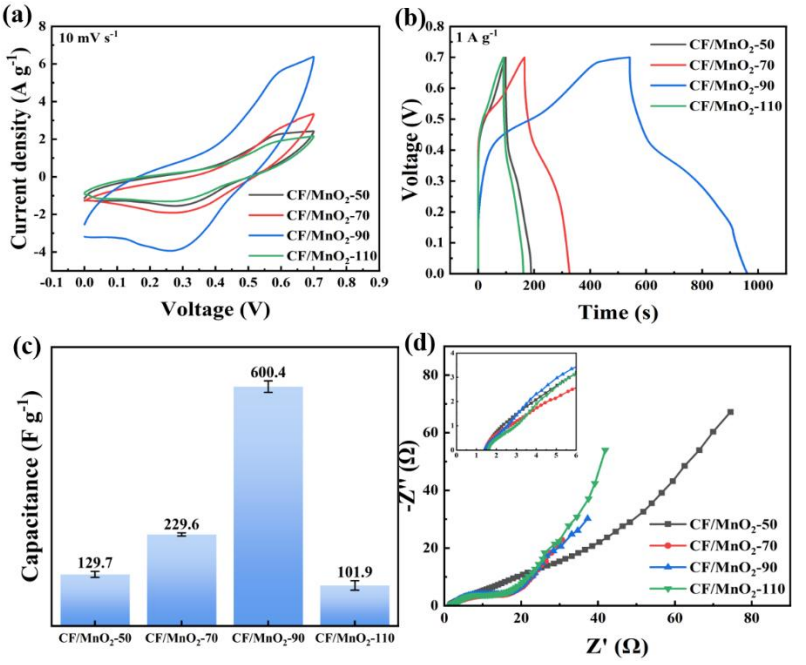

Fig. 5: (a) CV curves of CF/MnO_2 under varying reaction times at 10 mV s^{-1}, (b) GCD curves of CF/MnO_2 under varying reaction times at 1 A g^{-1}, (c) capacitance of CF/MnO_2 electrode for different reaction times at 1 A g^{-1}, and (d) EIS curves of CF/MnO_2 electrodes under varying reaction times.

curves of CF/MnO_2-70, CF/MnO_2-90 and CF/MnO_2-110 electrodes across various current densities., and similarly these above conclusions can be drawn.

Fig. 5(a) underscores CV curves for related electrodes within 0-0.7 V at 10 mV s^{-1}. The analysis indicates the CF/MnO_2-90 possesses the most extensive CV region, indicating its improved charge storage capacitance. The capacitance value of the CF/MnO_2-90 is determined to be of 335.71 F g^{-1}. In contrast, the specific capacitance values for the CF/MnO_2-50, CF/MnO_2-70, and CF/MnO_2-110 electrodes are respectively 62.86, 65, and 55.71 F g^{-1}. Fig. 5(b) illustrates GCD curves corresponding to various electrodes at 1 A g^{-1}. The capacitance value of the CF/MnO_2-90 is 600.4 F g^{-1}, while the capacitance of the CF/MnO_2-50, CF/MnO_2-70, and CF/MnO_2-110 are 129.7, 229.6, 101.9 F g^{-1}, which can be found from Fig. 5(c). GCD curves clearly depict the differences in discharge times for different samples. Fig. 5(d) presents the EIS curves for various electrodes, revealing a distinct observation that the transfer resistance of CF/MnO_2-50, CF/MnO_2-70, CF/MnO_2-90, and CF/MnO_2-110 electrodes

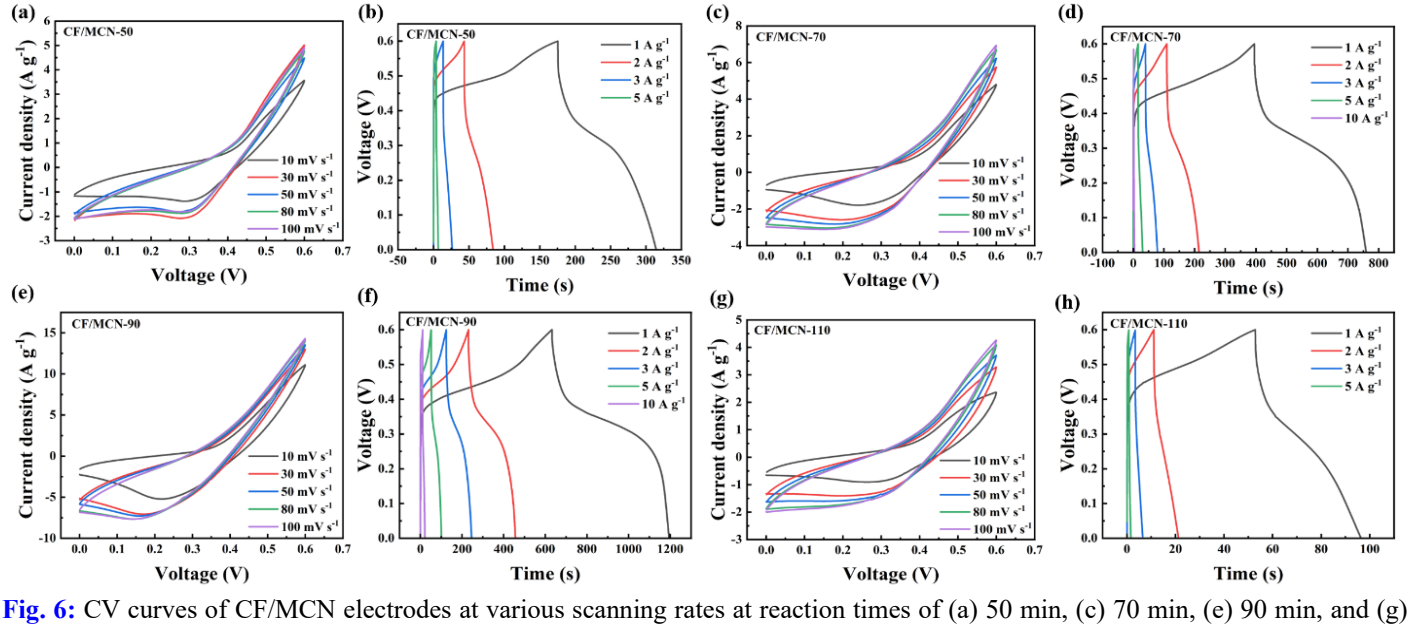

Fig. 6: CV curves of CF/MCN electrodes at various scanning rates at reaction times of (a) 50 min, (c) 70 min, (e) 90 min, and (g) 110 min, respectively, GCD curves of CF/MCN electrode at varying current densities at (b) 50 min, (d) 70 min, (f) 90 min, and (h) 110 min, respectively.

are 4.52, 4.14, 3.43, and 4.86 Ω, respectively, indicating the CF/MnO_2-90 has the best electrochemical properties.

In order to obtain a larger specific capacitance, CF/MCN was obtained by electrochemically depositing a layer of CoNi LDH onto the surface of CF/MnO_2-90, and the analysis on its electrochemistry property of the CF/MCN electrode was conducted, which is represented by Fig. 6. Fig. 6(a) illustrates CV curves of the CF/MCN-50 at various scan rates. Comparisons show that their configuration keeps largely consistent, which suggests a high degree of electrochemical reversibility and rapid ion transport. In addition, the existence of significant redox peaks at the values of 0.26 and 0.45 V suggests the appearance of a faraday redox reaction, which plays a critical role in enhancing the overall capacitance. Similarly, with the analysis of these three images in Figs. 6(c), (e) and (g), which represent the CV curves of CF/MCN-70, CF/MCN-90, and CF/MCN-110 electrodes at different scanning rates, it is concluded that their shape stays fundamentally the same, indicating exceptional electrochemical reversibility and high ion transport efficiency as above. Fig. 6(b) depicts the GCD curves of CF/MCN-50 electrode across various current densities. It shows a clear symmetry pattern and a clearly delineated voltage plateau, indicating a considerable capacitance for charge storage. Similarly, analyzing these three images of Figs. 6(d), (f) and (h), which represent GCD curves of CF/MCN-70, CF/MCN-90, and CF/MCN-110 electrodes at different current densities, shows a clear symmetry pattern and a clearly marked voltage plateau, also suggesting a notable capacitance for charge storage.

Fig. 7(a) presents the CV curves for CF/MCN electrode. The contrast exhibits the CF/MCN-90 has the widest CV region, indicating an improved charge storage capability. Its capacitance is 162.5 F g^{-1}, while the capacitance for the CF/MCN-50, CF/MCN-70, and CF/MCN-110 are separately found to be 46.7, 62.5, and 41.7 F g^{-1}. Fig. 7(b) illustrates GCD curves for these electrodes at 1 A g^{-1}. The capacitance for CF/MCN-90 electrode is calculated from the data to be up to 937.8 F g^{-1}, while the capacitance for the CF/MCN-50, CF/MCN-70, and CF/MCN-110 are 231.5, 608.3, and 72.2 F g^{-1} (Fig. 7(c)). GCD curves clearly depict the differences in discharge time for different samples. Fig. 7(d) presents the EIS curves for various electrodes, revealing a distinct observation that the electrode contacts resistances of CF/MCN-50, CF/MCN-70, CF/MCN-90, and CF/MCN-110 are 1.67, 1.84, 1.61, 2.24 Ω, respectively.

To highlight the superior performance of CF/MCN, CF/CoNi LDH electrodes are designed and electrochemically tested for comparison. Fig. 8 represents the electrochemical analysis test of CF/CoNi LDH electrode. Fig. 8(a) illustrates CV curves of the CF/CoNi LDH at different scan rates. Comparisons show the shapes of the curves are basically the same, but the change from 10 to 30 mV s^{-1} is larger, suggesting an enhancement in electrochemical reversibility and an improved ability for rapid ion transport., but it has a certain gap compared with the CF/MCN electrodes compared with CF/MCN electrodes. Fig. 8(b) depicts the GCD curves of CF/CoNi LDH electrode under varying current densities. It shows a more obvious symmetry and voltage plateau, indicating a better charge storage capability, but there is a gap compared with CF/MCN electrode. Fig. 8(c) presents the EIS curve of the CF/CoNi LDH electrode, and the resemblance of this curve to that of the CF/MCN electrode suggests that the CF/CoNi LDH electrode also exhibits superior electrochemical property.

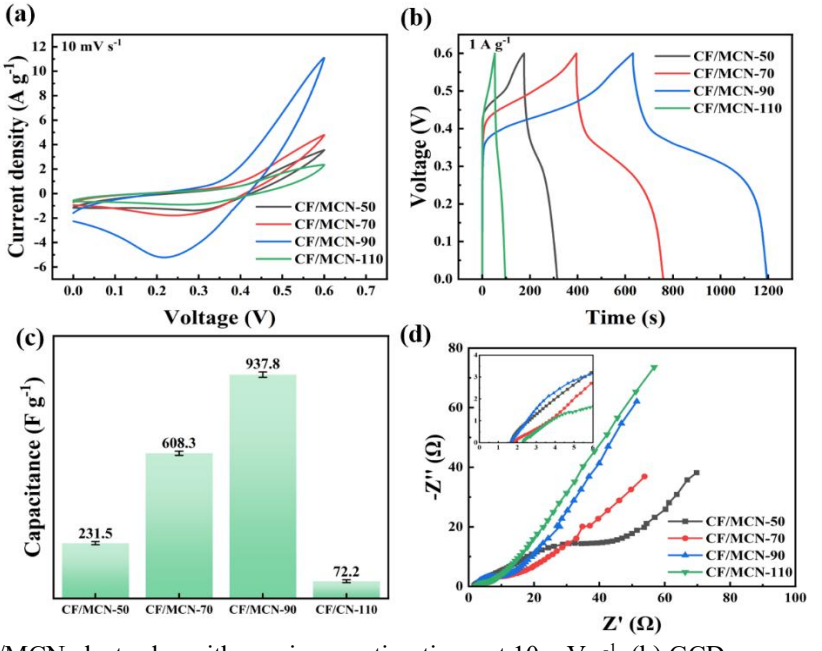

Fig. 7: (a) CV curves of CF/MCN electrodes with varying reaction times at 10 mV s^{-1}, (b) GCD curves of CF/MCN electrodes with varying reaction times at 1 A g^{-1}, (c) capacitance of CF/MCN electrodes with different reaction times at 1 A g^{-1}, (d) EIS curves of CF/MCN electrodes with different reaction times.

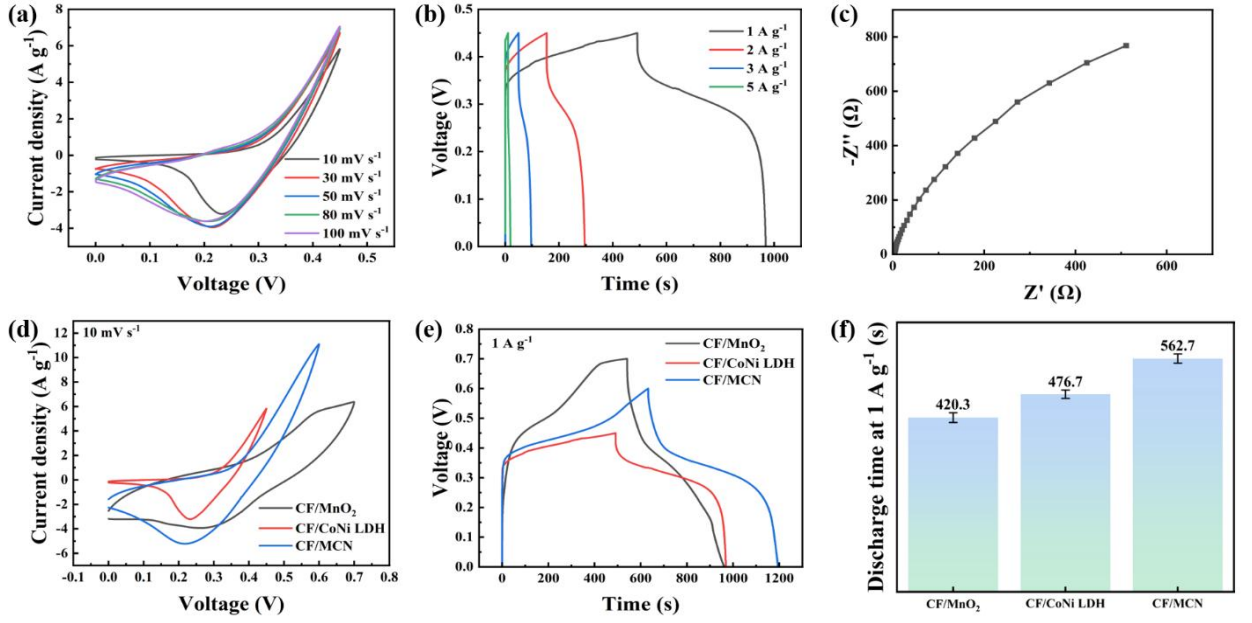

Fig. 8: (a) CV curves, (b) GCD curves, and (c) EIS curve of CF/CoNi LDH, (d) CV curves at 10 mV s^{-1}, (e) GCD curves at 1 A g^{-1}, and (f) discharge times of CF/MnO_2, CF/CoNi LDH, CF/MCN.

Fig. 8(d) highlights the contrast of CV curves for three electrodes (CF/MnO_2, CF/CoNi LDH and CF/MCN) at 10 mV s^{-1}. The comparative analysis reveals the CF/MCN has the most extensive CV region, signifying its superior ability for charge storage, and the CF/MnO_2 electrode also has a wider CV integration region, again indicating a higher charge storage capacitance. Fig. 8(e) shows GCD curves of the CF/MnO_2, CF/CoNi LDH and CF/MCN at 1 A g^{-1}. The specific capacitance values for the three electrodes have been determined from the data, yielding results of 600.4, 1059.3, and 937.8 F g^{-1}. The GCD curves distinctly illustrate the variations in discharge capacitance and voltage range among the different cases. Importantly, these differences considerably widen the operational voltage range for the electrodes, a phenomenon that can be ascribed to the doping of MnO_2. Fig. 8(f) presents the comparison about the discharge time of the three electrodes CF/MnO_2, CF/CoNi LDH and CF/MCN at 1 A g^{-1}. From the figure, it can be concluded that the discharge times of three electrodes, CF/MnO_2, CF/CoNi LDH and CF/MCN, are 420.3, 476.7, and 562.7 s, respectively, among which the CF/MCN electrode has the longest discharge duration, which indicates its superior electrochemical property.[35, 36]

To emphasize the practical importance of CF/MCN electrodes, a supercapacitor device with asymmetric pattern (MCN//AC) is constructed and subjected to a series of electrochemical tests as shown in Fig. 9. In this device, CF/MCN, CF/AC and PVA/KOH separately act as positive electrode, negative electrode, and gel electrolyte. Fig. 9(a) presents CV curves at 50 mV s^{-1} across various voltage windows ranging from 1.0 to 1.6 V. The data indicate this window extends up to 1.6 V without exhibiting distinct polarization at these elevated voltages. Fig. 9(b) illustrates its GCD curve with a voltage range spanning from 1.0 to 1.6 V, measured at 1 A g^{-1}. CV and GCD curves exhibit minimal variation from 1.0-1.6 V, indicating that the assembled device operates normally within this specified voltage range. Fig. 9(c) exhibits CV curves of the MCN//AC corresponding to varying scan rates. Their configuration remains relatively consistent with increasing scan rates, suggesting that the MCN//AC exhibits favorable rate capacitance. Furthermore, Fig. 9(d) represents the high symmetry of GCD curves of MCN//AC across 2-10 A g^{-1}, which proves that MCN//AC has remarkable capacitive characteristics. Fig. 9(e) displays the capacitance of MCN//AC under diverse scan rates. It is calculated that the specific capacitance values recorded at 10, 30, 50, 80, and 100 mV s^{-1} are respectively 90.6, 75, 66.9, 58.2, and 53.4 F g^{-1}. Fig. 9(f) illustrates the specific capacitance of MCN/AC across various current densities. It is calculated that the specific capacitance at 1, 2, 3, 5, 10 A g^{-1} is 151, 99.5, 83.8, 70.6 and 50 F g^{-1}. The calculation of CV and GCD indicates a slight reduction in capacitance at elevated scanning rates as well as high current densities. This outcome indicates that MCN//AC has good magnification performance, which can be ascribed to the rapid redox kinetics associated with the MCN//AC system. The device, operated under 800.02 W kg-1 power density, achieves 53.69 W h kg^{-1} energy density. The comparison between MCN//AC devices and previous work about voltage window, power density and energy density are depicted by Table 1, showing good development potential.[37-45] Fig. 9(g) shows the EIS plot and MCN//AC fitting data, and that the resistance to charge transfer is measured as 2.21 Ω. The diagram presented illustrates the equivalent circuit configuration that originates in the fitting procedure. The reduced resistance facilitates electron transport and significantly enhances electrochemical ability. Fig. 9(h) shows capacitance retention of the MCN//AC configuration following 10,000 cycles, and its value reaches 90.35% of the

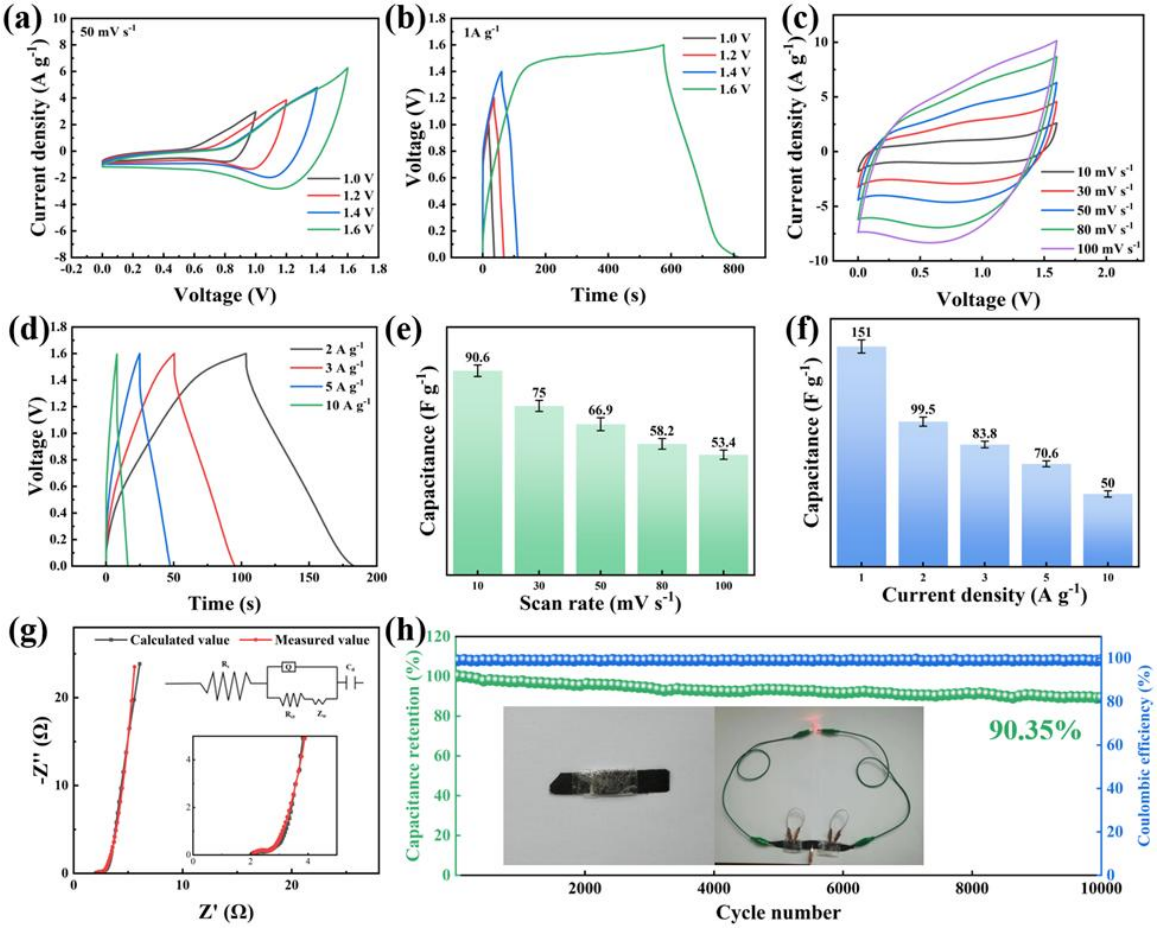

Fig. 9: (a) CV curves at 50 mV s^{-1} and (b) GCD curves at 1 A g^{-1} of MCN//AC for varying voltage windows, (c) CV curves with various scanning rate and (d) GCD curves with various current densities of of MCN//AC, capacitance of MCN//AC at (e) various scan rates and (f) various current densities, (g) EIS plot of MCN//AC and the equivalent circuit diagram, (h) capacitance retention and coulombic efficiency of the MCN//AC at 1 A g^{-1} for 10,000 cycles, and inset showing MCN//AC and two devices connected in series illumining a 1.8 V LED.

Table 1: Comparison of MCN//AC with previous work about potential window, power density and energy density.

Electrode	Potential window (V)	Power density (W kg^{-1})	Energy density (W h kg^{-1})	Ref.
LDH/rGO//rGO	1.6	772	34.5	[37]
NiAl-LDH//ACNF	1.5	750	20	[38]
$NiCo_2O_4$@CoFe-LDH//AC	1.7	950	28.94	[39]
LDH/rGO//rGO	1.6	400	29.3	[40]
NiAl-LDH/MXene//AC	1.7	255	27.6	[41]
CF-MX//AC	1.8	450	18.5	[42]
CNMV//V_2C	1.6	700	30.16	[43]
NCZ-LDH@PANI//AC	1.6	362	37.2	[44]
CF@(Ni, Co)Se_2//AC	1.6	800	36.02	[45]
MCN//AC	1.6	800.02	53.69	This work

initial state. After 10,000 cycles, coulombic efficiency remains almost 100%. The illustration shows that the device can effectively power a 1.8 V LED light, highlighting the excellent practical value of the supercapacitor device.

4. Conclusion

In summary, CF/MCN electrodes are prepared by in-situ growth technique as well as electrochemical deposition technique. The architecture of the prepared two-layer composite material efficiently utilizes the combined effect among the component substances, minimizes the ion transport distance, and improves the electrochemistry property of the electrode. At 1 A g^{-1}, the capacitance value of CF/MCN attains 937.8 F g^{-1}. A supercapacitor (CF/MCN//CF/AC) achieves 1.6 V voltage window. The capacitance measured at 1 A g^{-1} is 151 F g^{-1}. The device obtains 53.69 W h kg^{-1} energy density of while operating at 800.02 W kg^{-1} power density. After 10000 cycles, the device demonstrates 90.35% capacitance retention,

showing excellent cycle stability. In the future, MCN//AC devices are expected to present a strong and advantageous theoretical basis in relation to employing new environmentally sustainable devices.

Acknowledgments

We would like to thank Qiang Li from Shiyanjia Lab (www.shiyanjia.com) for the XPS analyses and we would like to thank eceshi (www.eceshi.com) for BET test.

Conflict of Interest

The authors declare that they have no conflict of interest.

Supporting Information

Not applicable.

References

[1] W. Luo, Y. Sun, Y. Han, J. Ding, T. Li, C. Hou, Y. Ma, Flexible $Ti_3C_2T_x$ MXene/polypyrrole composite films for high-performance all-solid asymmetric supercapacitors, *Electrochimica Acta*, 2023, **441**, 141818, doi: 10.1016/j.electacta.2023.141818.

[2] Y. Chen, I. H. Rowlands, The socio-political context of energy storage transition: Insights from a media analysis of Chinese newspapers, *Energy Research & Social Science*, 2022, **84**, 102348, doi: 10.1016/j.erss.2021.102348.

[3] Y. Liang, Z. Wei, X. Zhang, R. Wang, Fabrication of vanadium Oxide@Polypyyrole (V_2O_5@PPy) core-shell nanofiber electrode for supercapacitor, *ES Energy & Environment*, 2022, **18**, 101-110, doi: 10.30919/esee8c783.

[4] Z. Lin, L. Li, C. Xi, X. Li, S. Feng, C. Wang, H. Wang, T. Li, Y. Ma, Fabrication of the hollow dodecahedral NiCoZn layered double hydroxide for high-performance flexible asymmetric supercapacitor, *Journal of Colloid and Interface Science*, 2024, **657**, 91-101, doi: 10.1016/j.jcis.2023.11.139.

[5] A. V. Thakur, H. M. Pathan, B. J. Lokhande, Structural and electrochemical study of hybrid flexible electrodes containing *in situ* growth of RuO_2 within PPy matrix controlled by $RuCl_3$ % consumed during SILAR synthesis for preparation of symmetric device, *ES Energy & Environment*, 2022, **18**, 75-89, doi: 10.30919/esee8c751.

[6] Z. Li, J. Li, B. Wu, H. Wei, H. Guo, Z. M. El-Bahy, B. Liu, M. He, S. Melhi, X. Shi, S. D. Mekkey, Y. Sun, B. X. Ben, Z. Guo, Interfacial-engineered robust and high performance flexible polylactic acid/polyaniline/MXene electrodes for high-perfarmance supercapacitors, *Journal of Materials Science & Technology*, 2024, **203**, 201-210, doi: 10.1016/j.jmst.2024.02.084.

[7] Z. Sun, H. Qi, M. Chen, S. Guo, Z. Huang, S. Maganti, V. Murugadoss, M. Huang, Z. Guo, Progress in cellulose/carbon nanotube composite flexible electrodes for supercapacitors, *Engineered Science*, 2021, **18**, 59-74, doi: 10.30919/es8d588.

[8] R. Dhirendra Prasad, S. R. Prasad, R. Y. Prasad, C. P. I. A. N C, U. M. I. Bombay U, C. B. Desai, R. D. Kale, J. C. J. India, T. S. Bhat, S. U. K. India, O. P. Srivastava, S. Banga, A. Patil, B. Kamble, S. U. K. India, A. Kanthe, J. C. J. India, A. Saxena, D. C. K. India, S. Saxena, D. C. K. India, K. Saxena, D. C. K. India, P. Sarvalkar, S. U. K. India, A. K. Sharma, In memory of prin. RCP yadav, BVC Patna: a critical review on recent developments in advanced super-capacitors for veterinary medicine, *ES Food & Agroforestry*, 2022, **11**, 805, DOI: 10.30919/esfaf805.

[9] X. Li, H. Zhang, Z. Lin, Q. Liu, R. Li, J. Li, J. Ren, T. Li, Z. Sun, Y. Ma, Cobalt-nickel coordinated polyaniline as electrodes for high performance flexible asymmetric supercapacitor, *Journal of Energy Storage*, 2023, **72**, 108266, doi: 10.1016/j.est.2023.108266.

[10] X. Li, Z. Lin, C. Wang, H. Wang, S. Feng, T. Li, Y. Ma, Hierarchical graphene oxide/manganese dioxide/cobalt-nickel layered double hydroxide electrodes for high energy density asymmetric flexible supercapacitor, *Chemical Engineering Journal*, 2024, **484**, 149430, doi: 10.1016/j.cej.2024.149430.

[11] X. Li, Z. Lin, Y. Wei, W. Luo, J. Ding, T. Li, Y. Ma, MXene-MnO_2-CoNi layered double hydroxides// activated carbon flexible asymmetric supercapacitor, *Journal of Energy Storage*, 2022, **55**, 105668, doi: 10.1016/j.est.2022.105668.

[12] A. Mahmood, B. Zhao, M. S. Javed, D. He, W.-C. Cheong, D. Han, L. Niu, Unprecedented dual role of polyaniline for enhanced pseudocapacitance of cobalt-iron layered double hydroxide, *Macromolecular Rapid Communications*, 2022, **43**, e2100905, doi: 10.1002/marc.202100905.

[13] P. S. Jijoe, S. R. Yashas, H. PShivaraju, Fundamentals, synthesis, characterization and environmental applications of layered double hydroxides: a review, *Environmental Chemistry Letters*, 2021, **19**, 2643-2661, doi: 10.1007/s10311-021-01200-3.

[14] Q. Ma, X. Han, J. Cui, Y. Zhang, W. He, Ni embedded carbon nanofibers/Ni-Al LDHs with multicomponent synergy for hybrid supercapacitor electrodes, *Colloids and Surfaces A: Physicochemical and Engineering Aspects*, 2022, **649**, 129270, doi: 10.1016/j.colsurfa.2022.129270.

[15] W. Luo, Y. Ma, T. Li, H. K. Thabet, C. Hou, M. M. Ibrahim, S. M. El-Bahy, B. X. Ben, Z. Guo, Overview of MXene/conducting polymer composites for supercapacitors, *Journal of Energy Storage*, 2022, **52**, 105008, doi: 10.1016/j.est.2022.105008.

[16] X. Li, J. Ren, D. Sridhar, B. B. Xu, H. Algadi, Z. M. El-Bahy, Y. Ma, T. Li, Z. Guo, Progress of layered double hydroxide-based materials for supercapacitors, *Materials Chemistry Frontiers*, 2023, **7**, 1520-1561, doi: 10.1039/D2QM01346K.

[17] S. Li, Y. Luo, C. Wang, M. Wu, Y. Xue, J. Yang, L. Li, A novel hierarchical core-shell structure of $NiCo_2O_4$@NiCo-LDH nanoarrays for higher-performance flexible all-solid-state supercapacitor electrode materials, *Journal of Alloys and Compounds*, 2022, **920**, 165986, doi: 10.1016/j.jallcom.2022.165986.

[18] F. Chen, C. Chen, Q. Hu, B. Xiang, T. Song, X. Zou, W. Li, B. Xiong, M. Deng, Synthesis of CuO@CoNi LDH on Cu foam for high-performance supercapacitors, *Chemical Engineering Journal*, 2020, **401**, 126145, doi: 10.1016/j.cej.2020.126145.

[19] W. Wang, M. Zheng, J. Ren, M. Ma, X. Yin, T. Li, Y. Ma, Fabrication of magnetic $Fe_3O_4/MnO_2/TiO_2$/polypyrrole

heterostructure for efficient adsorption of Mn^{7+} from aqueous solution, *Journal of Applied Polymer Science*, 2022, **139**, 52199, doi: 10.1002/app.52199.
[20] Y. Ma, C. Hou, H. Zhang, Q. Zhang, H. Liu, S. Wu, Z. Guo, Three-dimensional core-shell Fe_3O_4/Polyaniline coaxial heterogeneous nanonets: Preparation and high-performance supercapacitor electrodes, *Electrochimica Acta*, 2019, **315**, 114-123, doi: 10.1016/j.electacta.2019.05.073.
[21] Y. Wei, M. Zheng, W. Luo, B. Dai, J. Ren, M. Ma, T. Li, Y. Ma, All pseudocapacitive MXene-MnO_2 flexible asymmetric supercapacitor, *Journal of Energy Storage*, 2022, **45**, 103715, doi: 10.1016/j.est.2021.103715.
[22] Y. Wei, W. Luo, Z. Zhuang, B. Dai, J. Ding, T. Li, M. Ma, X. Yin, Y. Ma, Fabrication of ternary MXene/MnO_2/polyaniline nanostructure with good electrochemical performances, *Advanced Composites and Hybrid Materials*, 2021, **4**, 1082-1091, doi: 10.1007/s42114-021-00323-z.
[23] W. Luo, Y. Sun, Z. Lin, X. Li, Y. Han, J. Ding, T. Li, C. Hou, Y. Ma, Flexible $Ti_3C_2T_x$ MXene/V_2O_5 composite films for high-performance all-solid supercapacitors, *Journal of Energy Storage*, 2023, **62**, 106807, doi: 10.1016/j.est.2023.106807.
[24] Y. Ma, Z. Zhuang, M. Ma, Y. Yang, W. Li, J. lin, M. Dong, S. Wu, T. Ding, Z. Guo, Solid polyaniline dendrites consisting of high aspect ratio branches self-assembled using sodium lauryl sulfonate as soft templates: Synthesis and electrochemical performance, *Polymer*, 2019, **182**, 121808, doi: 10.1016/j.polymer.2019.121808.
[25] Y. Li, B. Huang, X. Zhao, Z. Luo, S. Liang, H. Qin, L. Chen, Zeolitic imidazolate framework-L-assisted synthesis of inorganic and organic anion-intercalated hetero-trimetallic layered double hydroxide sheets as advanced electrode materials for aqueous asymmetric super-capacitor battery, *Journal of Power Sources*, 2022, **527**, 231149, doi: 10.1016/j.jpowsour.2022.231149.
[26] B. Dai, F. Dong, H. Wang, Y. Qu, J. Ding, Y. Ma, M. Ma, T. Li, Fabrication of CuS/Fe_3O_4@polypyrrole flower-like composites for excellent electromagnetic wave absorption, *Journal of Colloid and Interface Science*, 2023, **634**, 481-494, doi: 10.1016/j.jcis.2022.12.029.
[27] X. Hong, X. Wang, Y. Li, J. Fu, B. Liang, Sandwich structured MnO_2/carbon nanosheet/MnO_2 composite for high-performance supercapacitors, *Journal of Alloys and Compounds*, 2021, **889**, 161821, doi: 10.1016/j.jallcom.2021.161821.
[28] Q. Yang, Q. Wang, Y. Long, F. Wang, L. Wu, J. Pan, J. Han, Y. Lei, W. Shi, S. Song, *In situ* formation of Co_9S_8 quantum dots in MOF-derived ternary metal layered double hydroxide nanoarrays for high-performance hybrid supercapacitors, *Advanced Energy Materials*, 2020, **10**, 1903193, doi: 10.1002/aenm.201903193.
[29] B. Dai, F. Dong, J. Yu, S. Feng, H. Wang, T. Li, M. Ma, J. Ding, Y. Ma, Construction of Ni@polypyrrole nanochains/$Ti_3C_2T_x$ ternary composites with excellent microwave absorption properties, *Materials Chemistry Frontiers*, 2022, **6**, 3179-3192, doi: 10.1039/D2QM00672C.
[30] B. Dai, Y. Ma, F. Dong, J. Yu, M. Ma, H. K. Thabet, S. M. El-Bahy, M. M. Ibrahim, M. Huang, I. Seok, G. Roymahapatra, N. Naik, B. B. Xu, J. Ding, T. Li, Overview of MXene and conducting polymer matrix composites for electromagnetic wave absorption, *Advanced Composites and Hybrid Materials*, 2022, **5**, 704-754, doi: 10.1007/s42114-022-00510-6.
[31] Y. Wang, C. Shi, Y. Chen, D. Li, G. Wu, C. Wang, L. Guo, 3D flower-like MOF-derived NiCo-LDH integrated with $Ti_3C_2T_x$ for high-performance pseudosupercapacitors, *Electrochimica Acta*, 2021, **376**, 138040, doi: 10.1016/j.electacta.2021.138040.
[32] Z. Lin, X. Li, S. Li, B. Li, J. Ding, Y. Han, T. Li, C. Hou, Y. Ma, Highly flexible, foldable carbon cloth/MXene/polyaniline/CoNi layered double hydroxide electrode for high-performance all solid-state supercapacitors, *Journal of Energy Storage*, 2023, **64**, 107116, doi: 10.1016/j.est.2023.107116.
[33] Z. Ba, Y. Han, D. Qiao, D. Feng, G. Huang, Composite nanoparticles based on hydrotalcite as high-performance lubricant additives, *Industrial & Engineering Chemistry Research*, 2018, **57**, 15225-15233, doi: 10.1021/acs.iecr.8b02831.
[34] L. Zhu, C. Hao, X. Wang, Y. Guo, Fluffy cotton-like GO/Zn–co–Ni layered double hydroxides form from a sacrificed template GO/ZIF-8 for high performance asymmetric supercapacitors, *ACS Sustainable Chemistry & Engineering*, 2020, **8**, 11618-11629, doi: 10.1021/acssuschemeng.0c02916.
[35] C. Hou, W. Yang, X. Xie, X. Sun, J. Wang, N. Naik, D. Pan, X. Mai, Z. Guo, F. Dang, W. Du, Agaric-like anodes of porous carbon decorated with MoO_2 nanoparticles for stable ultralong cycling lifespan and high-rate lithium/sodium storage, *Journal of Colloid and Interface Science*, 2021, **596**, 396-407, doi: 10.1016/j.jcis.2021.03.149.
[36] L. E. Oloore, M. A. Gondal, A. Popoola, I. K. Popoola, Pseudocapacitive contributions to enhanced electrochemical energy storage in hybrid perovskite-nickel oxide nanoparticles composites electrodes, *Electrochimica Acta*, 2020, **361**, 137082, doi: 10.1016/j.electacta.2020.137082.
[37] K. Le, Z. Wang, F. Wang, Q. Wang, Q. Shao, V. Murugadoss, S. Wu, W. Liu, J. Liu, Q. Gao, Z. Guo, Sandwich-like NiCo layered double hydroxide/reduced graphene oxide nanocomposite cathodes for high energy density asymmetric supercapacitors, *Dalton Transactions*, 2019, **48**, 5193-5202, doi: 10.1039/C9DT00615J.
[38] W. Wang, N. Zhang, Z. Shi, Z. Ye, Q. Gao, M. Zhi, Z. Hong, Preparation of Ni-Al layered double hydroxide hollow microspheres for supercapacitor electrode, *Chemical Engineering Journal*, 2018, **338**, 55-61, doi: 10.1016/j.cej.2018.01.024.
[39] W. Chen, J. Wang, K. Y. Ma, M. Li, S. H. Guo, F. Liu, J. P. Cheng, Hierarchical $NiCo_2O_4$@Co-Fe LDH core-shell nanowire arrays for high-performance supercapacitor, *Applied Surface Science*, 2018, **451**, 280-288, doi: 10.1016/j.apsusc.2018.04.254.
[40] L. Huang, B. Liu, H. Hou, L. Wu, X. Zhu, J. Hu, J. Yang, Facile preparation of flower-like NiMn layered double hydroxide/reduced graphene oxide microsphere composite for high-performance asymmetric supercapacitors, *Journal of Alloys and Compounds*, 2018, **730**, 71-80, doi: 10.1016/j.jallcom.2017.09.195.

[41] J. Guo, Z. Bian, L. Ye, Y. Shang, F. Guo, Y. Zhang, J. Xu, Double layers combined with MXene and *in situ* grown NiAl-LDH arrays on nickel foam for enhanced asymmetric supercapacitors, *Ionics*, 2022, **28**, 2967-2977, doi: 10.1007/s11581-022-04520-8.
[42] R. Niu, R. Han, Y. Huang, L. Dai, H. Zhao, Y. Wang, J. Zhu, S. Tang, J. Sun, Hydrothermal ion exchange synthesis of CoM(M=Fe or Mn)/MXene 2D/2D hierarchal architectures for enhanced energy storage, *Journal of Alloys and Compounds*, 2022, **894**, 162385, doi: 10.1016/j.jallcom.2021.162385.
[43] Y. Zhang, J. Cao, J. Li, Z. Yuan, D. Li, L. Wang, W. Han, Self-assembled Cobalt-doped NiMn-layered double hydroxide (LDH)/V2CT x MXene hybrids for advanced aqueous electrochemical energy storage properties, *Chemical Engineering Journal*, 2022, **430**, 132992, doi: 10.1016/j.cej.2021.132992.
[44] N. C. Maile, M. Moztahida, A. A. Ghani, M. Hussain, K. Tahir, B. Kim, S. K. Shinde, V. J. Fulari, D. S. Lee, Electrochemical synthesis of binder-free interconnected nanosheets of Mn-doped Co_3O_4 on Ni foam for high-performance electrochemical energy storage application, *Chemical Engineering Journal*, 2021, **421**, 129767, doi: 10.1016/j.cej.2021.129767.
[45] Q. Yang, Y. Liu, C. Deng, L. Sun, W. Shi, *In-situ* construction of heterostructure (Ni, Co)Se_2 nanoarrays derived from cone-like ZIF-L for high-performance hybrid supercapacitors, *Journal of Colloid and Interface Science*, 2022, **608**, 3049-3058, doi: 10.1016/j.jcis.2021.11.036.